









Robust Beamforming with Gradient-based Liquid Neural Network

Xinquan Wang , Fenghao Zhu , Chongwen Huang , Ahmed Alhammadi , Faouzi Bader ,
Zhaoyang Zhang , Chau Yuen , *Fellow, IEEE*, and Mérouane Debbah , *Fellow, IEEE*

Abstract—Millimeter-wave (mmWave) multiple-input multiple-output (MIMO) communication with the advanced beamforming technologies is a key enabler to meet the growing demands of future mobile communication. However, the dynamic nature of cellular channels in large-scale urban mmWave MIMO communication scenarios brings substantial challenges, particularly in terms of complexity and robustness. To address these issues, we propose a robust gradient-based liquid neural network (GLNN) framework that utilizes ordinary differential equation-based liquid neurons to solve the beamforming problem. Specifically, our proposed GLNN framework takes gradients of the optimization objective function as inputs to extract the high-order channel feature information, and then introduces a residual connection to mitigate the training burden. Furthermore, we use the manifold learning technique to compress the search space of the beamforming problem. These designs enable the GLNN to effectively maintain low complexity while ensuring strong robustness to noisy and highly dynamic channels. Extensive simulation results demonstrate that the GLNN can achieve 4.15% higher spectral efficiency than that of typical iterative algorithms, and reduce the time consumption to only 1.61% that of conventional methods.

Index Terms—Beamforming, liquid neural networks, gradient, manifold learning, robustness.

I. INTRODUCTION

The sixth-generation (6G) is expected to incorporate a wide-range of communication capabilities that support an enriched and immersive experience, ensure ubiquitous coverage, and enable the new forms of collaboration. Millimeter-wave (mmWave) massive multiple-input multiple-output (MIMO) with the advanced beamforming technologies is recognized as a pivotal solution for 6G to enhance the system throughput [1]. However, new challenges come accompanying with the benefits of the mmWave MIMO technology, as mmWave channels are with high propagation loss and typically dominated by the line of sight (LoS) path. These factors result in a highly dynamic nature of mmWave channels in urban scenarios with

dense presence of small-scale obstacles such as vehicles [2]–[4], which makes it very hard to obtain the channel state information (CSI) accurately [5]. Therefore, designing an effective beamforming algorithm in large-scale urban mmWave MIMO communication scenarios has the substantial challenge.

To tackle with this challenge, several iterative methods have been introduced [6]–[8]. Specifically, [6] developed a dual-function scheme using semi-definite relaxation for robust beamforming performance. [7] pioneered the worst-case optimization, while [8] developed this approach with iterative precoders to improve robustness and reduce interference under conditions of imperfect CSI. However, the complexity of these methods increases greatly with more transmit antennas, challenging their applications in massive MIMO. Additionally, the impact mobility of the users has not been fully investigated.

On the other hand, some researchers have turned to the neural network (NN) based methods for their automatic feature extraction capabilities [9]–[16]. Specifically, [9] adopted deep reinforcement learning approaches that employ deep deterministic policy gradients to accommodate continuous action and state spaces. However, such approaches often incur high overhead. Recent studies [10]–[14] have explored deep NN models to reduce the overhead. However, their inherent structural limitations prevent them from capturing time domain information, which limits their effectiveness in processing highly dynamic mmWave channels. To address this challenge, an NN structure based on ordinary differential equations (ODEs) named liquid neural network (LNN) was introduced [15], [16]. Drawing inspiration from the nervous system of *Caenorhabditis elegans*, the LNN mimics the time-varying behavior of neural synapses, empowering the network with high capabilities in processing noisy continuous-time data.

In this paper, we proposed the gradient-based liquid neural network (GLNN) method to solve the beamforming problem in mmWave massive MIMO communication. This scheme combines manifold learning techniques and the LNN with a gradient-based learning approach to form a unified framework. Specifically, the ODE-based structure and the learnable parameters enables GLNN to effectively learn from noisy and dynamic CSI. The GLNN employs gradient-based learning to extract the high-order information from the inputs, while manifold learning significantly reduces the optimization space. This design allows the GLNN to achieve high performance and strong robustness to channel estimation errors with a compact NN. Unlike traditional NN-based methods, the GLNN only requires a short warm-up period instead of extensive pre-trainings as well. Simulation results demonstrate that the

X. Wang, F. Zhu, C. Huang and Z. Zhang are with the College of Information Science and Electronic Engineering, Zhejiang University, Hangzhou 310027, China (E-mails: {wangxinquan, zjuzfh, chongwen-huang, ning_ming}@zju.edu.cn).

A. Alhammadi and F. Bader are with Technology Innovation Institute, 9639 Masdar City, Abu Dhabi, UAE (E-mails: {Ahmed.Alhammadi, carlos-faouzi.bade}@tii.ae).

C. Yuen is with the School of Electrical and Electronics Engineering, Nanyang Technological University, Singapore 639798 (E-mail: chau.yuen@ntu.edu.sg).

M. Debbah is with KU 6G Research Center, Khalifa University of Science and Technology, P O Box 127788, Abu Dhabi, UAE and CentraleSupélec, University Paris-Saclay, 91192 Gif-sur-Yvette, France (E-mail: merouane.debbah@ku.ac.ae).

GLNN can achieve 4.15% higher spectral efficiency (SE) than that of typical iterative algorithms with as low as only 1.61% of the time consumption. To support further work, we have made our work open source at [17].

Notation: Scalars, vectors, and matrices are denoted by $a, \mathbf{a}, \mathbf{A}$, respectively. We denote transpose, Hermitian, inverse, L^2 norm, Hadamard product, modulus, computational complexity, expectation, determinant and trace as $\mathbf{A}^T, \mathbf{A}^H, \mathbf{A}^{-1}, \|\mathbf{A}\|_2, \odot, |\cdot|, \mathcal{O}, \mathbb{E}(\cdot), \det(\cdot), \text{Tr}(\cdot)$, respectively. All-zero and all-one vectors, and identity matrices are denoted as $\mathbf{0}, \mathbf{1}, \mathbf{I}$, respectively. We denote the complex Gaussian distribution as $\mathcal{CN}(\cdot, \cdot)$.

II. SYSTEM MODEL AND PROBLEM FORMULATION

In this section, we present the system model, and formulate the object maximization problem in mmWave massive MIMO communication.

Consider a downlink mmWave massive multi-user MIMO (MU-MIMO) communication system where a base station (BS) with M transmit antennas simultaneously serves K users, each of which are equipped with N_k receive antennas. The transmitted signal $\mathbf{u} \in \mathbb{C}^{M \times 1}$ can be represented as $\mathbf{u} \triangleq \mathbf{w}_k s_k$, where $\mathbf{w}_k \in \mathbb{C}^{M \times 1}$ denotes the precoding matrix for user k , and $s_k \in \mathbb{C}$ assumed as $s_k \sim \mathcal{CN}(0, 1)$ denotes the symbol intended for user k . We denote the channel matrix from the BS to the user k as $\mathbf{H}_k \in \mathbb{C}^{N_k \times M}$. The additive Gaussian noise vector as $\mathbf{n}_k \in \mathbb{C}^{N_k \times 1}$ with distribution $\mathcal{CN}(\mathbf{0}, \sigma^2 \mathbf{I})$, where σ^2 is the variance of the noise. Therefore, the received signal \mathbf{y}_k at user k can be expressed as

$$\mathbf{y}_k = \mathbf{H}_k \mathbf{w}_k s_k + \sum_{j=1, j \neq k}^K \mathbf{H}_k \mathbf{w}_j s_j + \mathbf{n}_k, \quad (1)$$

where the s_k and \mathbf{n}_k are assumed to be independent for different k . For clarity, we define $N \triangleq \sum_{k=1}^K N_k$ as the total number of receive antennas, and denote $\mathbf{y} \triangleq [\mathbf{y}_1^T, \mathbf{y}_2^T, \dots, \mathbf{y}_K^T]^T \in \mathbb{C}^{N \times 1}$, $\mathbf{W} \triangleq [\mathbf{w}_1, \mathbf{w}_2, \dots, \mathbf{w}_K] \in \mathbb{C}^{M \times K}$, $\mathbf{s} \triangleq [s_1, s_2, \dots, s_K]^T \in \mathbb{C}^{K \times 1}$, and $\mathbf{n} \triangleq [\mathbf{n}_1^T, \mathbf{n}_2^T, \dots, \mathbf{n}_K^T]^T \in \mathbb{C}^{N \times 1}$. We make a mild assumption that $\mathbf{H} \triangleq [\mathbf{H}_1^T, \mathbf{H}_2^T, \dots, \mathbf{H}_K^T]^T \in \mathbb{C}^{N \times M}$ has a full row rank. Therefore, (1) can be rewritten as $\mathbf{y} = \mathbf{H}\mathbf{W}\mathbf{s} + \mathbf{n}$.

In order to evaluate the robustness of algorithms with inaccurate channel information, we denote the estimated channel as $\hat{\mathbf{H}}$. We measure the accuracy of channel estimation with channel estimation error (CEE) in decibels (dB), which is defined as $\text{CEE} \triangleq 10 \log_{10} \left(\frac{\mathbb{E}[\|\mathbf{H} - \hat{\mathbf{H}}\|_2^2]}{\mathbb{E}[\|\mathbf{H}\|_2^2]} \right)$. This indicates that a lower CEE represents a more accurate channel estimation.

The SE of the system is given by

$$R = \sum_{k=1}^K \alpha_k R_k, \quad (2)$$

where the weight α_k represents the priority of user k . R_k denotes the achievable rate of the user k , which is given by

$$R_k \triangleq \log_2 \det \left(\mathbf{I} + \mathbf{H}_k \mathbf{w}_k (\mathbf{H}_k \mathbf{w}_k)^H \times \left(\sum_{j \neq k}^K \mathbf{H}_k \mathbf{w}_j (\mathbf{H}_k \mathbf{w}_j)^H + \sigma^2 \mathbf{I} \right)^{-1} \right). \quad (3)$$

The basic problem is to find an optimal \mathbf{W} with a constraint power that maximizes the SE of the system. In this paper, we use the sum power constraint (SPC) to limit the power of the transmit antennas, which is given as $\text{Tr}(\mathbf{W}\mathbf{W}^H) \leq P$, where P is the sum power budget of the transmit antennas. Under SPC, the problem can be formulated as

$$\begin{aligned} \max_{\mathbf{W}} \quad & R = \sum_{k=1}^K \alpha_k R_k \\ \text{s.t.} \quad & \text{Tr}(\mathbf{W}\mathbf{W}^H) \leq P. \end{aligned} \quad (4)$$

The function of SE is highly non-convex and non-linear, which makes the optimization problem (4) NP-hard [18].

III. GRADIENT-BASED LIQUID NEURAL NETWORK

In this section, we present the GLNN scheme which combines manifold learning techniques and LNN with a gradient-based learning approach to form a cohesive framework.

A. Manifold Learning Technique

For massive MU-MIMO communication system, the BS is usually equipped with a large number of transmit antennas. This makes the search space of the (4) extremely large, resulting in demanding and expensive training progress. Additionally, the number of transmit antennas at the BS is typically much larger than the number of receive antennas at the users [19]. Therefore, an efficient algorithm may have a search space that is independent of M [20]. Considering these factors, we utilize the manifold learning technique [10] to compress the search space for (4). With the help of the manifold learning technique, the optimal \mathbf{W} can be compressed as $\mathbf{W} = \mathbf{H}^H \mathbf{X}$, where $\mathbf{X} \in \mathbb{C}^{N \times K}$ is the base matrix for the optimal \mathbf{W} . Given $M \gg N$, this greatly reduces the search space from $\mathbb{C}^{M \times K}$ to a manifold of $\mathbb{C}^{N \times K}$. The proposed GLNN exploits this feature by optimizing the low-dimensional base matrix instead of optimizing the precoding matrix directly.

B. LNN Architecture

LNNs are networks that are constructed by linear first-order dynamical systems and controlled through nonlinear interconnected gates [15]. These networks are based on ODEs without the necessity for a solver and can model dynamical systems whose time constants are liquid in relation to their hidden states. A basic ODE can be expressed as

$$\frac{dp(t)}{dt} = -\frac{p(t)}{\tau} + S(t), \quad (5)$$

where $S(t) = f(i(t))(A - x(t))$ represents the synaptic current between neurons, and $p(t), A, \tau$ represents the hidden state, bias and time constant, respectively. To derive a closed-form solution, the hidden states of a layer of ODE-based liquid neurons can be determined by an initial value problem, which can be expressed as

$$\begin{aligned} \frac{d\mathbf{p}(t)}{dt} = & -[\mathbf{o}_\tau + \mathbf{f}(\mathbf{p}(t), \mathbf{i}(t), \theta) \odot \mathbf{p}(t)] \\ & + \mathbf{a} \odot \mathbf{f}(\mathbf{p}(t), \mathbf{i}(t), \theta), \end{aligned} \quad (6)$$

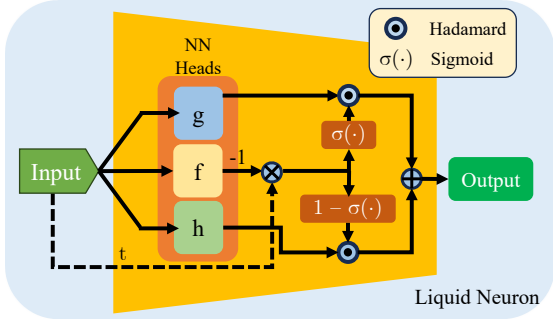


Fig. 1. Structure of a liquid neuron.

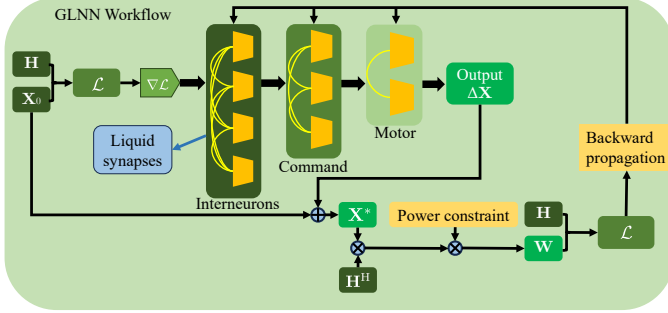


Fig. 2. Structure of GLNN.

where $\mathbf{p}(t) \in \mathbb{R}^{D \times 1}$, $\mathbf{i}(t) \in \mathbb{R}^{C \times 1}$, $\mathbf{o}_\tau \in \mathbb{R}^{D \times 1}$, $\mathbf{a} \in \mathbb{R}^{D \times 1}$, \mathbf{f} are the hidden states of a layer of D neurons (i.e. NN head), external inputs with C features, time constant parameter, bias and the function of the NN head with parameters θ_f , respectively. Given a continuous system described in (6), the closed-form solution can be approximated as

$$\begin{aligned} \mathbf{p}(t) &= (\mathbf{p}(0) - \mathbf{a}) \odot e^{-\mathbf{o}_\tau t - \int_0^t \mathbf{f}(\mathbf{i}(s), \theta_f) ds} + \mathbf{a} \\ &\approx \mathbf{b} \odot e^{-[\mathbf{o}_\tau + \mathbf{f}(\mathbf{i}(t), \theta_f)]t} \odot \mathbf{f}(-\mathbf{i}(t), \theta_f) + \mathbf{a}, \end{aligned} \quad (7)$$

where $(\mathbf{p}(0) - \mathbf{a})$ is denoted as $\mathbf{b} \in \mathbb{R}^{D \times 1}$ to allow explicit derivation of $\mathbf{p}(t)$. However, the exponential term in (7) causes the system to quickly converge to \mathbf{a} . To address this, we replace the exponential decay term with a smooth nonlinearity introduced by sigmoid gates. Finally, to enhance the flexibility of the GLNN, we have made both \mathbf{a} and \mathbf{b} trainable by replacing them with NN heads \mathbf{g} and \mathbf{h} , respectively. The closed-form continuous-time model for a layer of liquid neurons illustrated in Fig. 1 can be presented as

$$\begin{aligned} \mathbf{p}(t) &= \sigma(-\mathbf{f}(\mathbf{p}, \mathbf{I}; \theta_f)t) \odot \mathbf{g}(\mathbf{p}, \mathbf{I}; \theta_g) \\ &\quad + [\mathbf{1} - \sigma(-\mathbf{f}(\mathbf{p}, \mathbf{I}; \theta_f)t)] \odot \mathbf{h}(\mathbf{p}, \mathbf{I}; \theta_h), \end{aligned} \quad (8)$$

where θ_g, θ_h denote the parameters of NN heads with functions of \mathbf{g}, \mathbf{h} , respectively.

C. Gradient-based Optimization

Prior deep learning (DL)-based beamforming schemes typically feed the raw channel matrix \mathbf{H} into the NNs, and use the output directly as the precoding matrix \mathbf{W} . However, due to the high non-convexity of the optimization space, traditional NN-based architectures can hardly extract high-order information from the this space [10], [13], which can reduce the overall performance. To tackle with this, we introduce

Algorithm 1 GLNN Workflow

```

1: procedure GLNN( $\mathbf{H}$ )
2:   Randomly Initialize  $\theta, \mathbf{X}_0$ .
3:   Initialize  $\mathbf{W}_0$  by  $\mathbf{W}_0 = \mathbf{H}^H \mathbf{X}_0$ 
4:   for  $i \leftarrow 1, 2, \dots, N_e$  do
5:     Calculate  $\mathcal{L}_0$  with  $\mathbf{H}, \mathbf{W}_0$  by (10)
6:      $\Delta \mathbf{X} = \text{LNN}(\nabla \mathcal{L}_0, \theta)$ 
7:     Calculate  $\mathbf{W}$  by (9)
8:     Calculate the  $\mathcal{L}$  as (10)
9:     Calculate and record the  $R$  as (2)
10:    Update  $\theta$  as (11)
11:   end for
12:   return  $\mathbf{W}$ 
13: end procedure

```

the gradient-based optimization, which is a technique that feeds gradients of the optimization object into the NNs. This technique combines the ability of the NNs to extract time domain features of the optimization space with the high-order information extracted from the gradient-as-input mechanism, potentially leading to improved optimization performance. However, this combination may lead to difficulties in updating the parameters of the NNs. Inspired by the conception of residual learning technique in [21], we treats the output as the residual $\Delta \mathbf{X}$. This output is then used to update \mathbf{X} by $\mathbf{X}^* = \mathbf{X} + \Delta \mathbf{X}$, where \mathbf{X}^* denotes the updated base matrix.

D. GLNN Framework

This section introduces the GLNN framework as described in Algorithm 1 and Fig. 2

1) *Forward Propagation*: This procedure updates the precoding matrix. We first initialize the base matrix as \mathbf{X}_0 and calculate the loss function and its gradient with respect to \mathbf{X}_0 as $\nabla \mathcal{L} \in \mathbb{C}^{N \times K}$. Then we consider the $\nabla \mathcal{L}$ as a batch of vectors of dimension K and feed them into three layers of liquid neurons that are fully connected by liquid synapses, which named interneurons, command, and motor, respectively. Both the input and the output are decomposed into real and imaginary parts, thus both the interneurons layer and the motor layer contains $2K$ liquid neurons. Finally, considering the power constraints in (4), we can compute the precoding matrix as

$$\mathbf{W} = \sqrt{\frac{P}{\text{Tr}(\mathbf{H}^H \mathbf{X}^* (\mathbf{H}^H \mathbf{X}^*)^H)}} \cdot \mathbf{H}^H \mathbf{X}^*, \quad (9)$$

2) *Backward Propagation*: This procedure updates the LNN parameters. We noticed that NN-based algorithms usually have a tendency to provide signals to only one user, which introduces a fairness issue and limits the overall SE. Therefore, diverging from traditional methods that directly use $-R$ as the loss function, our strategy includes a penalty term to mitigate rate disparities among users by adding the variance of R_k for all users, denoted as $\text{Var}(R)$. To counterbalance the potentially excessive penalties from the penalty term that may hinder the optimization of GLNN, we introduce an incentive mechanism within our loss function. This mechanism initially encourages

the NN to undertake a straightforward search at the early stage, which prevents the network from overly prioritizing fairness and discouraging optimization efforts. The loss function can be denoted as

$$\mathcal{L} = -R + \beta \cdot \text{Var}(R) + \gamma \cdot \text{ReLU}(\lambda \cdot K - R), \quad (10)$$

where $\mathcal{L}, \beta, \gamma, \lambda$ denote the loss function, penalty rate, incentive rate and threshold, respectively. Then the backward propagation is conducted with Adam optimizer, as

$$\theta^* = \theta + \alpha \cdot \text{Adam}(\nabla_{\theta} \mathcal{L}, \theta), \quad (11)$$

where θ, θ^* are NN parameters $\{\theta_f, \theta_g, \theta_h\}$ before and after update, respectively, and α is the learning rate.

IV. SIMULATION RESULTS

In this section, we discuss the performance of the proposed GLNN method through simulation results. We construct the channel matrix using BS3 from scenario O1 of the open source DeepMIMO dataset [22] with parameters $M = 64, N_k = 2, K = 4, f_c = 28$ GHz, where f_c is the central frequency. We establish a warm-up period containing N_r samples for DL-based methods to learn knowledge from continuous samples over a period of time, and set $\alpha = 0.01, \beta = 0.3, \gamma = 0.7, \lambda = 2.5, N_e = 3, N_r = 500, \sigma^2 = 0$ dBm, $P = 10$ dBm as the default hyperparameters. The command layer in the GLNN comprises 30 liquid neurons. We generate 500 samples with continuously changing positions and average the results across all the samples. The inaccuracy of channel estimation $\hat{\mathbf{H}} - \mathbf{H}$ is assumed to follow a zero-mean white Gaussian distribution. We run all the simulations on a computer with an Intel i7-12700H CPU using Pytorch 2.1.2 and Python 3.11. We compare GLNN to several baselines as listed below.

- **Baseline 1 (WMMSE):** An iterative scheme from [23].
- **Baseline 2 (LAGD):** A DL-based model from [11].
- **Baseline 3 (LSTM):** A DL-based model employing a straightforward LSTM approach, directly mapping the $\hat{\mathbf{H}}$ to \mathbf{W} without the use of additional techniques.
- **Baseline 4 (Upper Bound):** To determine the potential maximal SE, we run the GLNN and all the baselines on perfect channel information sufficient times (i.e. 100 times) with independent random initialization and record the highest one as the upper bound.

A. Performance Evaluation

In this subsection, we evaluate the performance of the GLNN by comparing the SE with the baselines.

1) *Impact of P :* In Fig. 3, we present the SE of the proposed GLNN alongside the baselines under perfect channel information, under conditions of fixed σ^2 and varying P . The results show that the SE of all the algorithms increases with an increasing P , and the proposed GLNN outperforms all the baselines, being 4.15% higher than the WMMSE when P is 10 dBm. The underperformance of the LSTM and LAGD than the GLNN is due to design limitations. Specifically, the inability of the LSTM to effectively extract high-order information hampers optimization in complex spaces. Meanwhile, the absence of an ODE-based architecture in the LAGD reduces

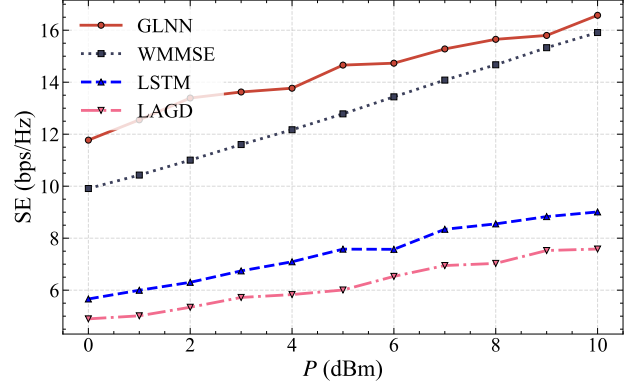


Fig. 3. SE vs. the transmit power under perfect channel information.

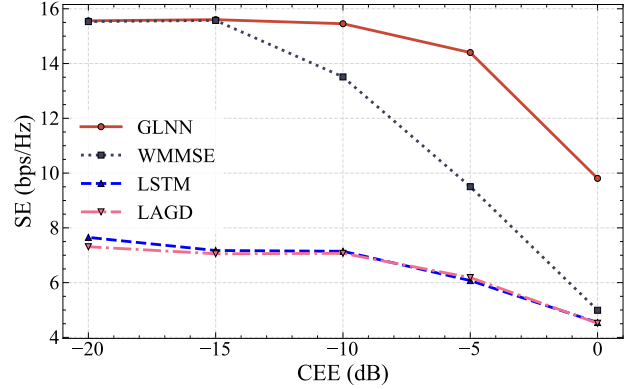


Fig. 4. SE vs CEE under $P = 10$ dBm.

its adaptability in dynamic scenarios, despite its theoretical capabilities in managing high-dimensional data.

2) *Impact of CEE:* In Fig. 4, we fix the P at 10 dBm and evaluate the performance of the algorithms as the CEE increases from -20 dB to 0 dB. The results show that both the WMMSE and the GLNN exhibit high SE at low CEE levels. However, while the WMMSE demonstrates reduced robustness against high CEE, the GLNN shows strong robustness, exhibiting a 96.59% higher SE at a CEE of 0 dB. This advantage is primarily due to its fully connected neural synapses and its ODE-based design, which allows GLNN to extract features from noisy inputs more effectively.

3) *Dynamic Scenarios:* In Fig. 5, we remove the warm-up phase for the LAGD, the LSTM and the GLNN and run all algorithms under a 10 dB CEE to more closely simulate real-world online performance. We provide three phases of speed, including 6 m/s, 15 m/s, and 30 m/s, with each phase comprising 700, 600, and 500 time slots, respectively. We smoothed the results in each phase for clarity. The GLNN model rapidly surpasses WMMSE after a short period and subsequently maintains higher SE over all baselines. Notably, the gap between the Upper Bound and the DL-based models widens as changing to phases of higher speeds. However, this increased gap swiftly closes as the GLNN adapts after just a few iterations, demonstrating its high adaptability and performance in dynamically changing environments. This is due to the multi-head design of liquid neurons in the GLNN, which replaces the bias and zero-state with trainable parameters and thus enables GLNN to adapt quickly to scenario changes.

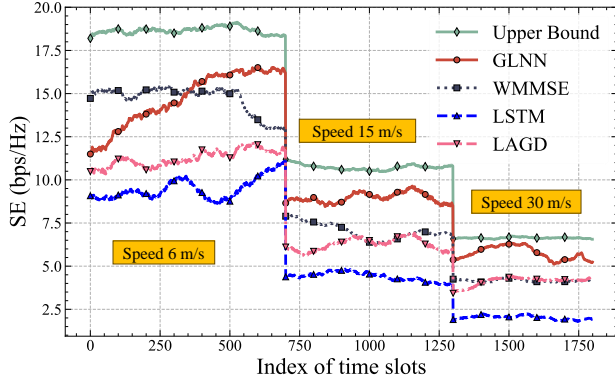


Fig. 5. Dynamic simulation results with CEE = -10 dB and without warm-up.

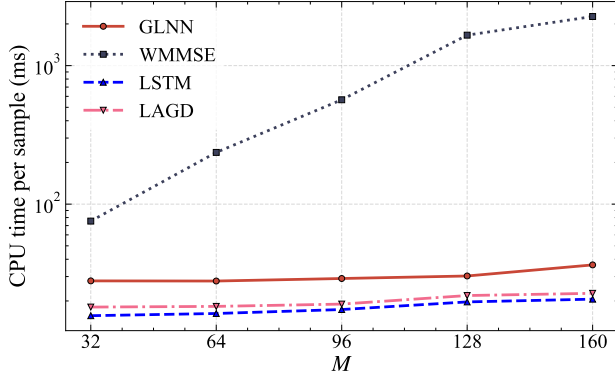


Fig. 6. Time for optimization with different M .

B. Time Consumption Evaluation

In this subsection, we compare the computational complexity of GLNN and the baseline algorithms as the number of BS transmit antennas increases. According to Fig. 6, the time cost of WMMSE rises rapidly with more antennas, while the rise of GLNN is slower, reaching a ratio of 1.61% compared to the WMMSE when $M = 160$. On the other hand, despite their lower complexity, LAGD and LSTM offer reduced SE, which limits their application. The main source of complexity in the GLNN are the LNN and the computation of R . The complexity of the LNN is $\mathcal{O}(NK)$, while the complexity of computing R is $\mathcal{O}(MNK + M^2K + N_k^3)$. Since these operations are repeated N_e times per sample, the total complexity of GLNN is $\mathcal{O}(N_e(MNK + M^2K + N_k^3))$. Table I provides a comparison of the computational complexity between GLNN and the baselines, where I_μ, I_W are the iteration numbers of the bisection searches and the three-step update loops in the WMMSE, respectively.

V. CONCLUSION

In this paper, a robust beamforming method named GLNN was presented. Specifically, the GLNN integrated the manifold learning technique and the ODE-based LNN with the gradient-based learning framework. Simulation results showed that the GLNN outperforms the baselines by 4.15%, and demonstrated the strong robustness against channel estimation inaccuracies while reducing the time consumption to only 1.61% that of conventional methods.

Table I
COMPARISON OF COMPUTATIONAL COMPLEXITY

Algorithm	Time Complexity
GLNN	$\mathcal{O}(N_e(MNK + M^2K + N_k^3))$
WMMSE	$\mathcal{O}(I_\mu I_W(MN^2 + MNK + M^3K^2 + NN_k^2))$
LAGD	$\mathcal{O}(N_e(M^2N + N_k^3))$
LSTM	$\mathcal{O}(N_e(MNK + M^2K + N_k^3))$

REFERENCES

- [1] C. Huang *et al.*, "Holographic MIMO surfaces for 6G wireless networks: Opportunities, challenges, and trends," *IEEE Wirel. Commun.*, vol. 27, no. 5, pp. 118–125, 2020.
- [2] W. Jiang *et al.*, "The road towards 6G: A comprehensive survey," *IEEE Open J. Commun. Soc.*, vol. 2, pp. 334–366, 2021.
- [3] B. Han, L. Wang, and H. D. Schotten, "A 3D human body blockage model for outdoor millimeter-wave cellular communication," *Phys. Commun.*, vol. 25, pp. 502–510, 2017.
- [4] T. Gong *et al.*, "Holographic MIMO communications with arbitrary surface placements: Near-field LoS channel model and capacity limit," *IEEE J. Sel. Areas Commun.*, pp. 1–1, 2024.
- [5] W. Xu *et al.*, "Robust beamforming with partial channel state information for energy efficient networks," *IEEE J. Sel. Areas Commun.*, vol. 33, no. 12, pp. 2920–2935, 2015.
- [6] B. Liao, X. Xiong, and Z. Quan, "Robust beamforming design for dual-function radar-communication system," *IEEE Trans. Veh. Tech.*, vol. 72, no. 6, pp. 7508–7516, 2023.
- [7] H. Shen *et al.*, "A worst-case robust MMSE transceiver design for nonregenerative mimo relaying," *IEEE Trans. Wirel. Commun.*, vol. 13, no. 2, pp. 695–709, 2013.
- [8] V. M. Palhares, A. R. Flores, and R. C. De Lamare, "Robust MMSE precoding and power allocation for cell-free massive mimo systems," *IEEE Trans. Veh. Tech.*, vol. 70, no. 5, pp. 5115–5120, 2021.
- [9] C. Huang *et al.*, "Multi-hop RIS-empowered terahertz communications: A DRL-based hybrid beamforming design," *IEEE J. Sel. Areas Commun.*, vol. 39, no. 6, pp. 1663–1677, 2021.
- [10] F. Zhu *et al.*, "Robust beamforming for RIS-aided communications: Gradient-based manifold meta learning," [Online] available: <https://arxiv.org/abs/2402.10626>, Feb. 2024.
- [11] Z. Yang *et al.*, "A learning-aided flexible gradient descent approach to MISO beamforming," *IEEE Wirel. Commun. Lett.*, vol. 11, no. 9, pp. 1895–1899, 2022.
- [12] F. Zhu *et al.*, "Robust millimeter beamforming via self-supervised hybrid deep learning," in *2023 31st Eur. Signal Process. Conf. (EUSIPCO)*. IEEE, 2023, pp. 915–919.
- [13] X. Wang *et al.*, "Energy-efficient beamforming for RISs-aided communications: Gradient based meta learning," in *Proc. 2024 IEEE Int. Conf. Commun. (ICC)*, Jun. 2024.
- [14] F. Zhu *et al.*, "Beamforming inferring by conditional WGAN-GP for holographic antenna arrays," [Online] available: <https://arxiv.org/abs/2405.00391>, Feb. 2024.
- [15] R. Hasani *et al.*, "Closed-form continuous-time neural networks," *Nat. Mach. Intell.*, vol. 4, no. 11, pp. 992–1003, 2022.
- [16] M. Chahine *et al.*, "Robust flight navigation out of distribution with liquid neural networks," *Sci. Robot.*, vol. 8, no. 77, p. eadc8892, 2023.
- [17] X. Wang, "GLNN," <https://github.com/tp1000d/GLNN>, 2024.
- [18] Z.-Q. Luo and S. Zhang, "Dynamic spectrum management: Complexity and duality," *IEEE J. Sel. Topics Signal Process.*, vol. 2, no. 1, pp. 57–73, 2008.
- [19] E. Björnson *et al.*, "Massive MIMO is a reality—what is next?: Five promising research directions for antenna arrays," *Digit. Signal Process.*, vol. 94, pp. 3–20, 2019.
- [20] X. Zhao *et al.*, "Rethinking WMMSE: Can its complexity scale linearly with the number of BS antennas?" *IEEE Trans. Signal Process.*, vol. 71, pp. 433–446, 2023.
- [21] K. He *et al.*, "Deep residual learning for image recognition," in *Proc. IEEE Conf. Comput. Vis. Pattern Recognit. (CVPR)*, 2016, pp. 770–778.
- [22] A. Alkhateeb, "Deepmimo: A generic deep learning dataset for millimeter wave and massive MIMO applications," in *Proc. of Information Theory and Applications Workshop (ITA)*, San Diego, CA, Feb 2019, pp. 1–8.
- [23] Q. Shi *et al.*, "An iteratively weighted MMSE approach to distributed sum-utility maximization for a MIMO interfering broadcast channel," *IEEE Trans. Signal Process.*, vol. 59, no. 9, pp. 4331–4340, Sept. 2011.